

Re-Estimated Effects of Deep Episodic Slip on the Occurrence and Probability of Great Earthquakes in Cascadia

by N. M. Beeler, Evelyn Roeloffs, and Wendy McCausland

Abstract [Mazzotti and Adams \(2004\)](#) estimated that rapid deep slip during typically two week long episodes beneath northern Washington and southern British Columbia increases the probability of a great Cascadia earthquake by 30–100 times relative to the probability during the ~ 58 weeks between slip events. Because the corresponding absolute probability remains very low at $\sim 0.03\%$ per week, their conclusion is that though it is more likely that a great earthquake will occur during a rapid slip event than during other times, a great earthquake is unlikely to occur during any particular rapid slip event. This previous estimate used a failure model in which great earthquakes initiate instantaneously at a stress threshold. We refine the estimate, assuming a delayed failure model that is based on laboratory-observed earthquake initiation. Laboratory tests show that failure of intact rock in shear and the onset of rapid slip on pre-existing faults do not occur at a threshold stress. Instead, slip onset is gradual and shows a damped response to stress and loading rate changes. The characteristic time of failure depends on loading rate and effective normal stress. Using this model, the probability enhancement during the period of rapid slip in Cascadia is negligible ($< 10\%$) for effective normal stresses of 10 MPa or more and only increases by 1.5 times for an effective normal stress of 1 MPa. We present arguments that the hypocentral effective normal stress exceeds 1 MPa. In addition, the probability enhancement due to rapid slip extends into the interevent period. With this delayed failure model for effective normal stresses greater than or equal to 50 kPa, it is more likely that a great earthquake will occur between the periods of rapid deep slip than during them. Our conclusion is that great earthquake occurrence is not significantly enhanced by episodic deep slip events.

Introduction

The plate boundary between North America and the subducting Juan de Fuca plate, extending from Cape Mendocino in northern California to northern Vancouver Island in British Columbia, has a Global Positioning Systems (GPS)-inferred convergence rate of between 45 and 39 mm/yr ([Dragert *et al.*, 2001](#)). The plate boundary is presently almost entirely aseismic, and the strain accumulation inferred from GPS data suggests an approximately 60×1000 km wide band of the plate interface is locked (e.g., [Dragert *et al.*, 1994](#); [Burgette *et al.*, 2009](#), also see [McCaffrey *et al.*, 2000, 2007](#); [Mazzotti *et al.*, 2003](#)). From the areal extent of the locked region, paleoseismic evidence of coastal subsidence events ([Atwater, 1987](#); [Atwater and Hemphill-Haley, 1997](#); [Witter *et al.*, 2003](#); [Leonard *et al.*, 2004](#)), and turbidites in marine sediment cores ([Adams, 1990](#); [Goldfinger *et al.*, 2012](#)), it is believed that this boundary fails in great thrust earthquakes with estimated mean recurrence of between 500 and 600 years ([Adams, 1990](#); [Goldfinger *et al.*, 2003](#); [Witter *et al.*, 2003](#)). The most recent event is thought to have generated an earth-

quake-induced tsunami recorded in Japan on 26 January 1700 ([Satake *et al.*, 1996](#)) and to have a magnitude approaching M_w 9. The extensive recent work by [Goldfinger *et al.* \(2012\)](#) narrows the range of average recurrence of these largest events in Cascadia to 500–530 years. The 500 year recurrence for M_w 8.8 to M_w 9 events in Cascadia used in the most recent U.S. Geological Survey (USGS) National Seismic Hazards Map ([Petersen *et al.*, 2008](#)) and the Uniform California Earthquake Rupture Forecast (UCERF), version 2 ([Frankel and Petersen, 2008](#)), reflects the prevailing view based on Goldfinger's studies. Given the long recurrence interval and relatively short elapsed time since the last event, 50 year conditional probabilities for end-to-end ruptures of the subduction zone that tacitly assume a constant rate of loading are relatively small at 5%–14% ([Adams and Weichert, 1994](#); [Petersen *et al.*, 2008](#); [Goldfinger *et al.*, 2012](#)), with the larger values being associated with the more recent studies. The 30 year conditional probability from the UCERF study is 10% ([Working Group on California Earthquake Probabilities,](#)

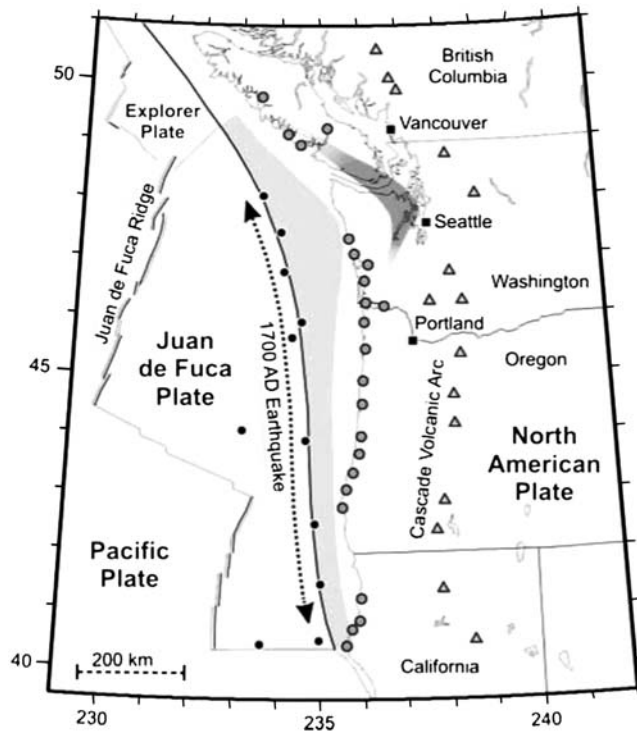


Figure 1. Schematic map of Cascadia from [Mazzotti and Adams \(2004\)](#). The approximate location of the trench is marked by the black line. Down-dip and east of the trench is the locked portion of the subduction interface that is expected to slip in the next great earthquake (light gray). Farther down-dip, beneath northern Washington and southern British Columbia, is the approximate location of the episodic slow-slip events ([Dragert et al., 2001](#)), as inferred from GPS data (darker gray). The Cascade volcanoes, marked by triangles, lie even farther to the east. To the west are the oceanic plate boundaries. Black circles are the locations of offshore turbidite samples used to constrain great earthquake recurrence ([Goldfinger et al., 2003](#)). The locations with paleoseismological evidence for onshore coastal subsidence attributed to recurring great earthquakes ([Leonard et al., 2004](#)) are marked by the shaded circles. The figure is used with permission.

2008), and this value is consistent with the USGS National Maps.

Recent high-resolution GPS shows, however, that the loading of the locked zone does not occur at a constant rate. Instead, at quasiperiodic intervals, slip accelerates to approximately three times the long-term rate over a portion of the deep extension of the subduction zone beneath Vancouver Island, down-dip of the inferred locked zone ([Dragert et al., 2001](#)). The approximate locations of the locked zone and slipping zone underneath Vancouver Island are shown in Figure 1. As was initially inferred from located nonvolcanic tremor ([McCausland et al., 2005](#)) and subsequently measured directly by GPS and borehole strain ([Brudzinski and Allen, 2007](#); [Szeliga et al., 2008](#); [Roeloffs et al., 2009](#); [Schmidt and Gao, 2010](#)), episodes of accelerated slip at depth occur farther south than shown in Figure 1, as well as independently in other locations in Washington, Oregon, and northern California within the Cascadia subduction

zone, and the average durations of accelerated slip episodes in Cascadia vary along strike.

Presumably, the locked portion of the subduction interface beneath Vancouver Island is loaded more rapidly during these periods of fast deep slip, potentially affecting the timing of great earthquakes. In Cascadia, the Geological Survey of Canada (GSC) and the USGS are the agencies responsible for estimating seismic hazard. It is a stated goal of both agencies to monitor and understand the significance of fast slip for the probability of the next great Cascadia earthquake. Stephane Mazzotti and John Adams of the GSC produced the first revised estimates that account for variable deep slip rate and concluded that during periods of fast slip the probability is enhanced approximately 50 times ([Mazzotti and Adams, 2004](#)). To estimate the effects of variable loading rate due to deep slip, [Mazzotti and Adams \(2004\)](#) assumed that beneath Vancouver Island the average slip event lasts two weeks and recurs every 14 months. Their estimate, however, is based on a threshold earthquake failure model that assumes an earthquake occurs when shear stress reaches a critical value. As we discuss in more detail below, for a threshold failure model, the earthquake recurrence interval is inversely proportional to the loading rate.

In contrast to the threshold failure model, laboratory rock friction and failure studies suggest an intrinsic time delay characterizes the short-term response of faults to changes in loading rate (e.g., [Scholz, 1968](#); [Dieterich, 1979](#)). Under slow rates of loading, the time delay greatly reduces any change in seismicity rate that might result from a change in loading rate. In the present study, we use such a laboratory-based fault failure criterion and reconsider the probability of the great Cascadia earthquake during and between periods of accelerated deep slip.

To estimate the relation between transient deep accelerated slip and great earthquake probability using a delayed failure model, in the following sections the solutions for some simpler underlying problems are developed. That is, the Cascadia result is built incrementally from the solutions for changes in the occurrence time of an individual earthquake resulting from changing the loading rate, then for changes in earthquake rate resulting from changes in loading rate, and finally for the effect of periodic changes in loading rate on the occurrence of a great earthquake. In the next section, after a short description of the laboratory evidence for delayed failure, the initial solutions for changes in the failure time of an individual earthquake and for populations of earthquakes are described. The [Application to Earthquake Recurrence](#) section considers the specific case of earthquake recurrence in which earthquake rate is a probabilistic rate—a probability density function—and applies the resulting solution to periodic changes in loading rate in Cascadia.

A complexity in interpretation that arises with delayed failure models is that the delay itself depends strongly and nonlinearly on the effective normal stress. Because normal stress is not well known in Cascadia, this introduces considerable uncertainty to our estimates, as is described in some detail

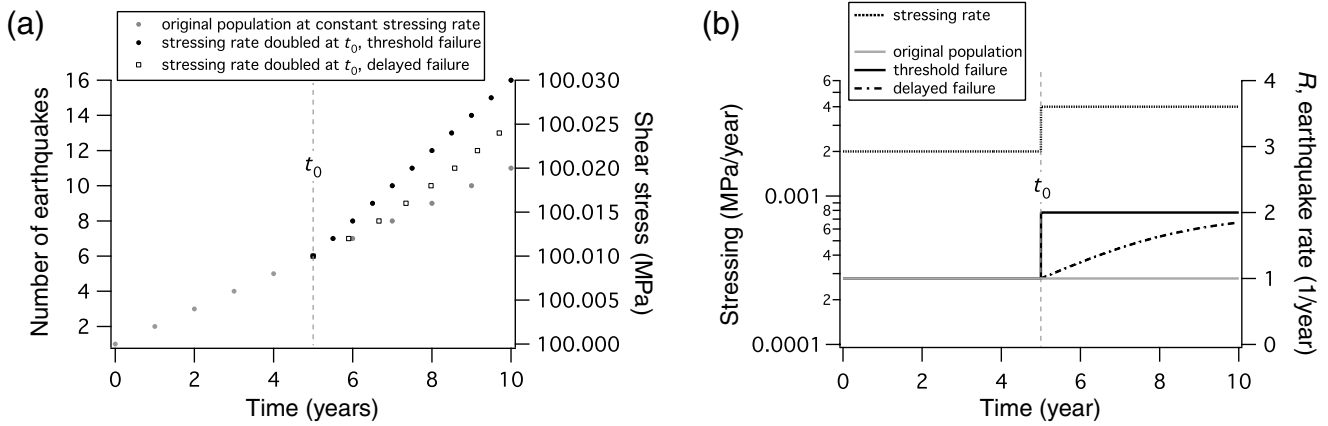


Figure 2. The response of seismicity to an increase in stressing rate. (a) The solid gray circles depict the failure times of individual earthquakes at a constant seismicity rate of one earthquake/year over a period of 10 years. The stressing rate is $\dot{\tau}_0 = 0.002$ MPa/yr, and the stress is shown on the right axis. After five years (t_0), if the stressing rate is doubled to 0.004 MPa/yr, the black symbols show the failure times of a threshold model. The open squares are a delayed failure model with characteristic time $t_a = 2$ years (see text). (b) The stressing rate (dashed line starting at 2 MPa/yr on left axis) and seismicity rates (right axis) associated with the case shown in (a).

in the [Discussion](#). Other limitations to our calculations and needs for additional research are also described. Those caveats notwithstanding, we argue that effective normal stress exceeds 1 MPa in the hypocentral region of the pending great Cascadia earthquake, which, if true, reduces the probability enhancement due to transient deep slip to insignificant levels.

Estimating the Effect of Changing Loading Rate on Earthquake Occurrence

Imagine a hypothetical collection of faults whose initial stress states are such that while being loaded at a constant rate results in a seismicity rate—the number of faults failing per unit time—that is constant. This case is shown graphically in Figure 2. In Figure 2a, each solid gray circle represents the failure strength (right axis) and failure time of an earthquake. The failure strengths are equally spaced in stress. The question we wish to address in this study is what happens to the seismicity rate if the stressing rate is changed. Obviously, in the absence of actual data, the answer to this question is speculation that will depend on the assumed sensitivity of the fault population to changes in loading rate. For a threshold failure relation such as Coulomb failure, the seismicity rate changes in exact proportion to the change in stressing rate, as follows: according to the Coulomb criterion, failure occurs the instant shear stress on the fault reaches the critical value τ_c ,

$$\tau_c = C + f\sigma_e, \quad (1a)$$

in which C and f are cohesion and the friction coefficient, respectively, and σ_e is the effective normal stress. With reference to Figure 2, at constant normal stress, constant loading rate and constant initial seismicity rate, r_0 , doubling of the stressing rate at time t_0 (Fig. 2a), decreases the remaining time to failure for each fault (solid black symbols, Fig. 2a) by the ratio of the new loading rate $\dot{\tau}_1$ to the original rate $\dot{\tau}_0$. The

loading rate (left axis) and resulting seismicity rate (right axis) corresponding to the individual failure times in Figure 2a are shown in Figure 2b. The new seismicity rate r_1 is

$$r_1 = r_0 \frac{\dot{\tau}_1}{\dot{\tau}_0} \quad (1b)$$

(black trace, Fig. 2b). Equation (1b) is time independent reflecting the time independence of the failure criterion in (1a). (Table 1 contains a list of all variables used in this article.)

Our eventual solutions for great earthquake occurrence will resemble the general form of equation (1b), namely, $r_1 = r_0 g(\dot{\tau}_1/\dot{\tau}_0)$, the product of an initial earthquake rate with a function g that depends on the ratio of the stressing rates; however, the eventual solutions will differ from equation (1b) in two significant ways. First, in the remainder of this section, we consider a delayed failure model. This leads to an earthquake rate equation in which the stressing rate ratio in (1b) is replaced with a function that is time dependent, $g(\dot{\tau}_1/\dot{\tau}_0, t)$. Second, in the [Application to Earthquake Recurrence](#) section, we will modify the conceptual model of a hypothetical collection of faults, used to construct the earthquake rate equation (1b), to instead represent possible failure times of the Cascadia subduction fault. To do so, we replace the initial earthquake rate in (1b) with a probability density function, resulting in a time-dependent probabilistic estimate of the occurrence time of the next great earthquake.

In contrast to equation (1a), modern laboratory experiments indicate intact rock and rock friction stick-slip failures are time dependent. The time dependence is well illustrated in a set of static fatigue tests (e.g., [Scholz, 1972](#); [Kranz, 1980](#); Fig. 3). Figure 3 shows measurements of the failure stress of individual laboratory faults versus time to failure. Each point represents an individual experiment on an intact sample of granite that is raised to a particular stress level and held at that level until failure occurs. Not only does failure occur at different stress levels, but there also can be an

Table 1
List of Variables Used in This Article

Variable	Definition	Equation Number or Location in Text
a	Frictional rate dependence coefficient	(2a)
b	Frictional weakening coefficient	(2a)
C	Cohesion	(1a)
d	Distance from source	Discussion
d_c	Slip-weakening distance	(2a)
f	Friction coefficient	(1)
f_*	Nominal friction coefficient	(2)
f'	Effective friction coefficient	Discussion
G	Shear modulus	Table 2
k	Fault shear stiffness	(A3)
N	Number of earthquakes	Application to Earthquake Recurrence
n	Earthquake sequence number	Appendix B
n_T	Total number of earthquakes	Appendix C
p	Probability density function	(C1)
P	Probability distribution	Application to Earthquake Recurrence
P_c	Conditional probability	Application to Earthquake Recurrence
P_{rw}	Probability that earthquakes are uncorrelated with tides	(3)
P_{rapid}	Cumulative probability during a period of rapid slip	Discussion
P_{slow}	Cumulative probability between periods of rapid slip	Discussion
r_1	Seismicity rate	(1b)
r_0	Initial seismicity rate	(1b)
s	Standard deviation	(C1)
t	Time	(below A3)
t_a	Time constant governing the time evolution of V and r	(1b)
t_{tf}	Time to failure	(A3)
t_f	Time of failure	(below A3)
t_f^0	Time of failure at initial loading rate	(A4)
t_f^1	Time of failure at modified loading rate	(A4)
t_r	Recurrence interval	(C1)
t_{start}	Start time of rapid-slip period	Discussion
t_{end}	End time of rapid-slip period	Discussion
t_0	Time at which loading rate changes	(A4)
V	Slip velocity	(2a)
V_*	Reference slip velocity	(2a)
W	Fault width	Discussion
δ	Fault slip	(2a)
δ_L	Loading displacement	(above A3)
ϕ	Dip angle of fault	(4)
γ	“Shape factor” in inverse Gaussian probability density	(C1)
μ	Average recurrence interval	(C1)
σ_e	Effective normal stress	(1a)
σ_L	Lithostatic stress	(4)
σ_n	Fault-normal stress	(4)
τ	Shear stress	(4)
τ_c	Coulomb stress	(1a)
$\dot{\tau}_1$	Modified stressing rate	(1b)
$\dot{\tau}_0$	Initial stressing rate	(1b)
$\Delta\tau$	Tidal stress amplitude	(3)
$\Delta\tau_s$	Static stress drop	(Table 2)

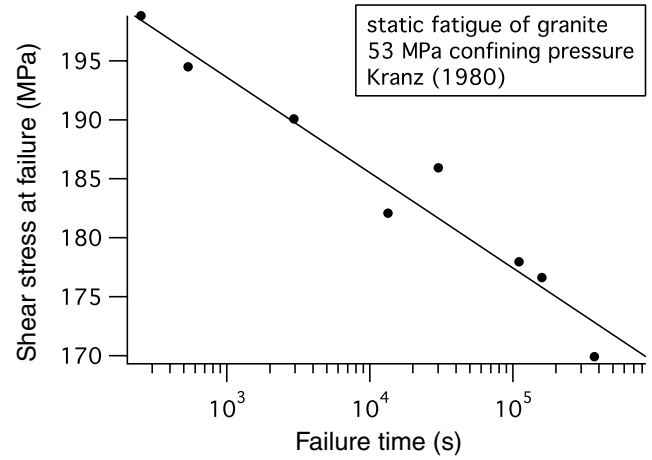


Figure 3. Time-dependence of earthquake initiation measured in rock failure tests. Experimental static fatigue data from rock fracture of granite at 53 MPa confining pressure (Kranz, 1980). In a static fatigue test, stress on the rock sample is raised and held at a particular value until failure occurs. Each point represents a single experiment. Failure stress was estimated from the reported differential stress data, assuming a 30° angle between the greatest principal stress and the incipient failure plane. For the delayed failure model in equation (2), a fit to this dataset yields $a\sigma_e = 3.5$ MPa. The mean fault normal stress in these tests is 426 MPa, implying $a = 0.008$.

extremely long delay between attaining a particular stress level and the actual time of failure. This manifestation of delayed failure characterizes failure of ceramics and metals as well as of rock.

Because the failure times and stresses at failure vary systematically, a time-independent threshold model (equation 1a) cannot reproduce the fundamental fault properties seen in the static fatigue tests (Fig. 3) or in other delayed failure tests described in more detail below. For time-dependent failure, instead of using equations (1a) and (1b), fault strength can be described by

$$\tau = \sigma_e \left(f_* + a \ln \frac{V}{V_*} - b \frac{\delta}{d_c} \right) \quad (2a)$$

(Dieterich, 1992, 1994), in which δ is slip, σ_e is the effective normal stress, and τ is shear stress in the direction of slip. V is slip rate, presumed in this model to always be nonzero across the failure plane or the pre-existing fault; a and b are experimentally determined and are second order relative to the nominal friction coefficient f_* ; V_* is a reference slip velocity; and d_c is a slip weakening distance. Equation (2a) states that, for a given effective stress, the shear stress at failure increases with increasing slip speed, and decreases with accumulated slip.

The solution to the slip- and rate-dependent strength equation (2a) for a static fatigue test (black line in Fig. 3, solution given as equation A2 in Appendix A) well captures the time-dependent failure seen in the tests, namely a logarithmic dependence of stress at failure on failure time. The slope in Figure 3 is the product $a\sigma_e \ln(10)$, indicating that the

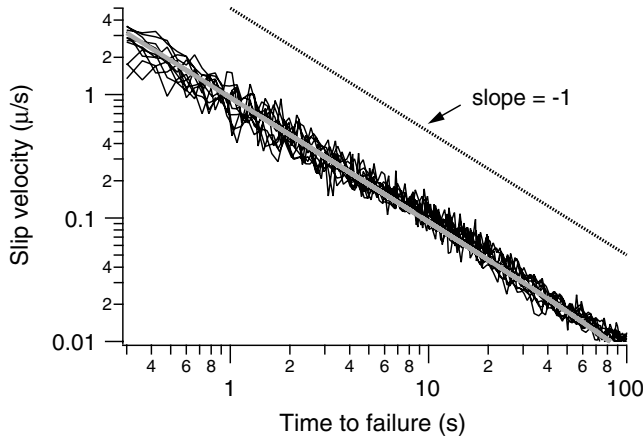


Figure 4. Time dependence of earthquake initiation, measured in stick-slip friction tests. Delayed failure from 11 successive stick-slip events of a pre-existing fault surface of Sierra granite at 4 MPa normal stress, loaded at a constant stressing rate of 0.0001 MPa/s. The plot shows the on-fault slip velocity versus time to failure (Kilgore and Beeler, 2010, after Dieterich, 1992). The dotted reference line shows a slope of -1 . The heavy gray line is the prediction from the delayed failure model in equation (2), with $a = 0.008$, $b = 0.01$, $\sigma_n = 4$ MPa, $d_c = 3.3$ μm , and $k = 0.0033$ MPa/ μm .

$a\sigma_e \ln V/V_*$ term in (2a) is the rheological element entirely responsible for delayed failure in this model (Dieterich, 1992, 1994).

Although static fatigue tests isolate some aspects of the delay, because the experimental procedure involves holding the fault at a constant stress level, they are a poor experimental analog for natural tectonic loading in which the stress level is usually assumed to increase slowly at an approximately constant rate due to the motion of the Earth's tectonic plates. A better laboratory analog for natural earthquake occurrence is frictional sliding on a pre-existing fault that is loaded to failure at a constant stressing rate. Figure 4 shows the variation of slip rate as the failure is approached in time (time to failure decreases from right to left) for 11 recurrences of stick slip on a single large laboratory fault (Kilgore and Beeler, 2010, after Dieterich and Kilgore, 1996). The imposed shear-stressing rate is 0.0001 MPa/s, and normal stress is 4 MPa. Failure is preceded by slip that accrues over hundreds of seconds at this loading rate as the fault gradually accelerates to failure (e.g., Dieterich, 1992; Dieterich and Kilgore, 1996). This gradual onset of rapid slip is well characterized by the failure model (equations 2a, 2b). By representing the interaction of the fault with the elastic surroundings using a single degree-of-freedom elastic element, predicted failure time for an arbitrary stressing history can be calculated (Dieterich, 1994). The solution for failure time resulting from constant loading rate is given as equation (A3) in Appendix A, and the heavy gray line in Figure 4 is a prediction of equations (2a), (2b) for these laboratory conditions and fault properties.

As was the case for the static fatigue tests (Fig. 3), the predicted delay of failure for equations (2a) and (2b) for constant rate loading results from the $a\sigma_e \ln V/V_*$ term

(Dieterich, 1992, 1994; see Appendix A). The characteristic relaxation time of this term for a change in stressing rate is, $t_a = a\sigma_e/\dot{\tau}$ (Beeler, 2004). The temporal significance of t_a is that it is approximately the duration of the nucleation of failure (Dieterich, 1992). Equivalently, t_a is the time period over which equations (2a) and (2b) differ from the instantaneous, threshold failure relation in equations (1a) and (1b). For the simulation of failure due to constant rate loading that is shown in Figure 4 (heavy gray line), t_a is 400 s.

If, instead of constant rate loading, the stressing rate is subsequently changed at some time t_0 from an initial stressing rate $\dot{\tau}_0$ to $\dot{\tau}_1$, then the predicted failure time will also change. This is shown in Figure 2a (open squares), in which the individual failures at times greater than $t_0 = 5$ years are subject to a change in loading rate by a factor of 2. The failure time of each earthquake had the loading rate not been changed is indicated by the gray symbols. The solution for failure time is derived in Appendix A (equation A4). Furthermore, because failure is inherently time dependent with the model in equations (2a) and (2b), the size of the change in failure time will depend on how close to failure the fault was when the new loading rate was applied. So, the predicted seismicity rate, r_1 , following a change in loading rate is time dependent (Fig. 2b). The solution for an initially constant seismicity rate r_0 , subject to an imposed change in stressing rate for a population of faults, derived in Appendix B (equation B2), is

$$r_1 = r_0 \frac{\exp\left(\frac{t-t_0}{t_a}\right)}{1 - \frac{\dot{\tau}_0}{\dot{\tau}_1} + \frac{\dot{\tau}_0}{\dot{\tau}_1} \exp\left(\frac{t-t_0}{t_a}\right)}. \quad (2b)$$

A comparison of delayed failure (equation 2b; dashed-dotted line in Fig. 2b) to threshold failure (equation 1b; black in Fig. 2b) for a change in stressing rate shows that rather than the instantaneous change, the seismicity rate evolves gradually. It will eventually approach the steady-state value $r_0\dot{\tau}_1/\dot{\tau}_0$ over a few relaxation times t_a .

Estimates of t_a in the shallow crust under hydrostatic effective normal stress are many years to decades. For example, in a strike-slip setting such as the San Andreas plate boundary using $a = 0.008$ and a stressing rate of 2.75 MPa/100 year at depths between 5 and 15 km using an effective normal stress gradient of 18 MPa/km, t_a would be between 26 and 79 years. Previously published estimates of t_a are of this order. Parsons *et al.* (2000) found $t_a \sim 25$ years for 12 $M_w \geq 6.7$ North Anatolian earthquakes, and $t_a = 7$ –11 years for 100 $M_w \geq 7$ global events (Parsons, 2002), most of which struck on subduction megathrusts. Toda *et al.* (2005) found $t_a = 25$ –52 years for the Landers earthquake and 66 years for the Hector Mine earthquake. Based on these examples and given the short duration of the deep rapid slip events in Cascadia relative to t_a , we would expect much smaller changes in probability for delayed failure than for threshold failure. In the next section, we show this by applying both models to estimate the effects of periodic loading on the occurrence of a great Cascadia earthquake.

Application to Earthquake Recurrence

The above predictions for a single change in stressing rate can be applied to the case of episodic changes in loading rate, such as those seen in Cascadia, by considering successive changes in loading rate. In the following calculations, we use periodic changes to idealize the observed quasiperiodic changes in stressing rate from deep slip. An additional consideration beyond the case described by equations (1b) and (2b), in which the earthquake rate remains constant in the absence of a change in stressing rate, is that we wish to consider the more general case of a background earthquake rate that is intrinsically time varying. It has been shown in a number of previous studies (Stein *et al.*, 1997; Hardebeck, 2004; Beeler *et al.*, 2007) that cases of nonconstant seismicity rate can be dealt with by replacing the constant background earthquake rate r_0 (in equations 1b or 2b) by a time varying rate $r_0(t)$ (also see Appendix B).

In particular, to estimate changes in the rate of great Cascadia earthquakes we have a probabilistic representation of the earthquake recurrence time (Mazzotti and Adams, 2004), a density function with average recurrence and variance. In the following analysis, we represent the earthquake probability density with an inverse Gaussian distribution (see Appendix C). The inverse Gaussian is an arbitrary choice, and our eventual conclusions do not depend on the choice of density function. The previous studies by Hardebeck (2004) and Beeler *et al.* (2007) dealt with changes in a probabilistic representation of recurrence resulting from changes in stress in the same manner as in the current study. Relevant details and specific solutions for a change in loading rate are included in Appendix C.

Cascadia

A great deal more information about deep accelerated slip and large earthquake occurrence in Cascadia has come to light since the Mazzotti and Adams (2004) study was published. Mazzotti and Adams (2004) presumed that deep slip below Vancouver Island influenced great earthquake occurrence times. In effect, they assumed that great Cascadia earthquakes nucleate up-dip from this portion of the subduction zone. Subsequently it has been learned that episodic deep slip occurs not only beneath Vancouver Island, but also independently at different locations along Cascadia at other times (S. Mazzotti, GSC, personal comm., 2009; Mazzotti, 2007; Szeliga *et al.*, 2008; Roeloffs *et al.*, 2009). Slip at these other locations presumably also influences great earthquake occurrence. In an unpublished revision of Mazzotti and Adams (2004) that accounts for the lateral extension and segmentation of episodic slip, Mazzotti (2007) finds five times lower probability amplification during episodic slip events than in the original study. The refined recurrence interval of great earthquakes is now shorter at 500–530 years (Frankel and Petersen, 2008; Petersen *et al.*, 2008; Goldfinger *et al.*, 2012) than used in the original study, resulting in

larger 50 year conditional probabilities. However, it is now more widely acknowledged that large earthquake occurrence in Cascadia is segmented with smaller M_w 8 events restricted to southern Cascadia occurring between the great Cascadia events and having shorter recurrences of ~ 240 years (Goldfinger *et al.*, 2012). Segmentation of deep slip and large earthquakes will only serve to reduce the Mazzotti and Adams (2004) probability estimates (e.g., Mazzotti, 2007). Here, we will ignore the complications of segmented episodic slip and segmented large earthquake occurrence and make a direct comparison with Mazzotti and Adams (2004) to see how consideration of delayed failure changes probability estimates. As we show below, we find that periodic deep rapid slip does not produce a significant enhancement of the great earthquake probability.

To estimate earthquake probability in Cascadia due to nonconstant loading from deep slip, we undertake a single representative calculation following Mazzotti and Adams (2004). Accordingly, the average stressing rate is inferred from assuming average large earthquakes recur approximately every 600 years and typically have a stress drop of 3 MPa (the median value for subduction zone earthquakes of Allmann and Shearer, 2009), which results in a stressing rate of 0.005 MPa/yr. The deep slip episodes beneath Vancouver Island typically last about two weeks and recur, approximately, every 60 weeks (Mazzotti and Adams, 2004). Slip during the two weeks of rapid slip accounts for only 65% of the total subduction convergence in the region (Mazzotti and Adams, 2004). Combining these constraints, representative rates of stressing during a deep slip event and during the interevent time are 0.09 MPa/yr and 0.002 MPa/yr, respectively.

Threshold Failure

For threshold failure, the amplitude of the probability density is modulated by the ratio of the rapid deep slip loading rate to the interevent rate, a factor of about 50 (Fig. 5a,b). This calculation, detailed in Appendix C, repeats Mazzotti and Adams (2004), the principal difference being in the choice of density function. An inverse Gaussian distribution is used rather than a Gaussian distribution so that the probability at $t_r = 0$ is strictly zero. The probability that an earthquake will occur before time t_r is $P(t_r) = \int_0^{t_r} p(t_r) dt_r$. The conditional probability P_c , the probability that an earthquake will occur before time t_r , given that it has not yet occurred at time t_s , is $P_c(t_r) = [P(t_r) - P(t_s)]/[1 - P(t_s)]$ (Savage, 1991). For threshold failure, conditional probabilities for nonconstant loading due to periodic accelerated deep slip are modulated by the ratio of the rapid deep-slip loading rate to the interevent loading rate (Fig. 5c), just as they modulate the density function. Thus, the conditional probability that a great earthquake will occur during a two week period of accelerated deep slip, is about 50 times greater than it is during interevent periods (Mazzotti and Adams, 2004).

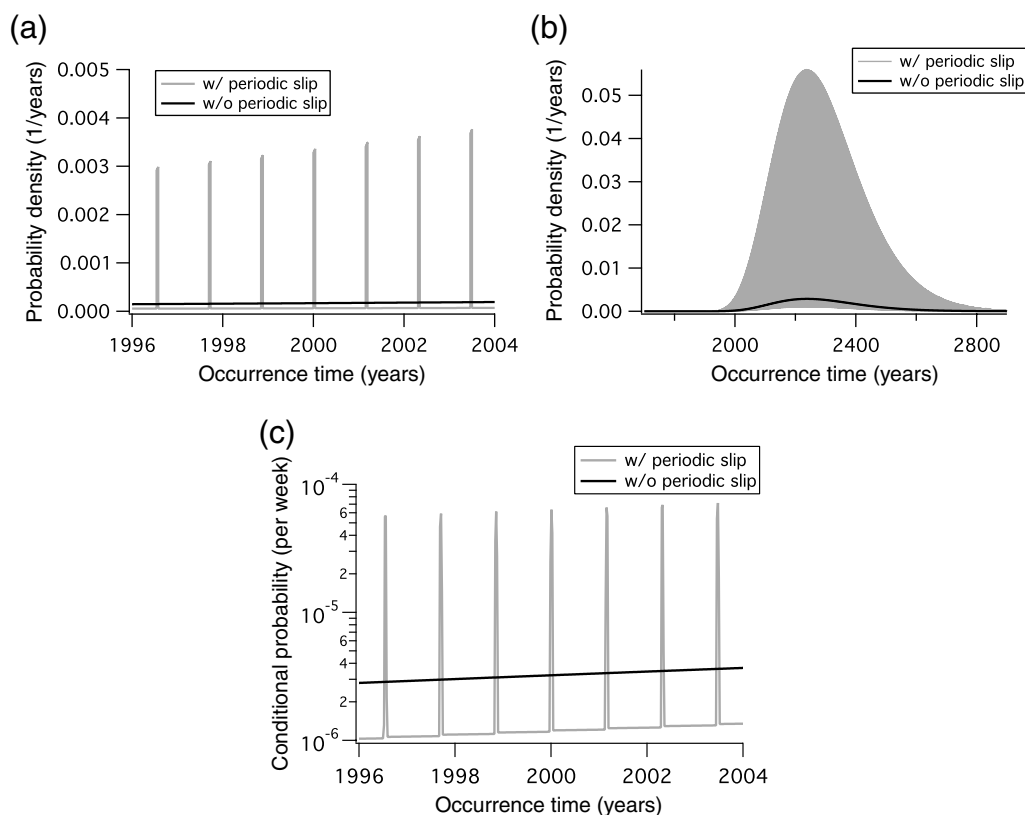


Figure 5. Comparison of the expected probability of a great Cascadia earthquake, assuming a threshold failure relation, subject to constant loading (black) and to periodic loading (gray). (a) The inverse Gaussian probability density is shown, with mean of 592.5 years and standard deviation of 149.3 years. These values are the maximum likelihood values from offshore turbite-inferred occurrences as summarized in [Mazzotti and Adams \(2004\)](#). The black lines indicate the occurrence density, assuming constant loading rate of 0.0045 MPa/yr. The case in gray assumes periodic loading with fast loading of 0.089 MPa/yr for two weeks with interevent slow loading at 0.0017 MPa/yr for 58 weeks. Probability values oscillate between the upper and lower bounds with a 60 week period. (b) The probability density in (a) is shown at a reduced scale. The wide gray swath is an artifact resulting from plotting the highly variable probabilities shown in (a) but at a compressed timescale. (c) The one week conditional probability calculated for the result shown in (a).

Delayed Failure

At room temperature, the laboratory-derived friction parameter a that controls the time delay has values between 0.003 and 0.013 (e.g., [Beeler et al., 2007](#)). In the following calculations we use $a = 0.008$, appropriate for quartzofeldspathic material at room temperature. The resulting density distribution is time dependent with a much lower amplitude change associated with the stressing rate change than for threshold failure (compare with Figs. 5a and 6d). The amplitude of the rate change depends strongly on normal stress (Fig. 6a–c); these calculations span three orders of magnitude in normal stress. For normal stresses of 100 and 10 MPa, there is effectively no change in the probability density despite a factor of 50 change in loading rate. The reason is that the delay time constant t_a is 8.96 and 0.896 years, whereas the duration of the increased loading is only 0.038 years. Only when the time constant is of the same order as or smaller than the duration of the fast loading, is there noticeable amplification, for example, at 1 MPa normal stress at which the time constant is 0.0896 years. However, even at this very low effective normal stress the resulting maximum in the probability density is only

a factor of 1.5 larger than the minimum of the density at the slower loading rate (Fig. 7a). Even if the amplification by 1.5 was in effect throughout the two weeks of faster loading, the conditional probability would only be increased by a factor of 1.5, which, given the small absolute value of the conditional probability, is not significant. Furthermore, as follows from the simpler rate-change calculations (Fig. 2), because the result is time dependent (Fig. 6d), the amplified seismicity rate during the period of fast loading does not immediately vanish when the event is over, but instead decays slowly during the interevent period, so that the interevent period is not entirely a time of lower earthquake probability.

Discussion

For our spatially dimensionless model of Cascadia earthquake probability, whether episodic deep slip influences earthquake failure time depends on (1) the choice of failure relation (e.g., equations 1a and 1b or 2a and 2b) and, (2) the hypocentral effective normal stress. In the following discussion, we emphasize the physical reasoning why delayed failure is the more appropriate failure relation to use when

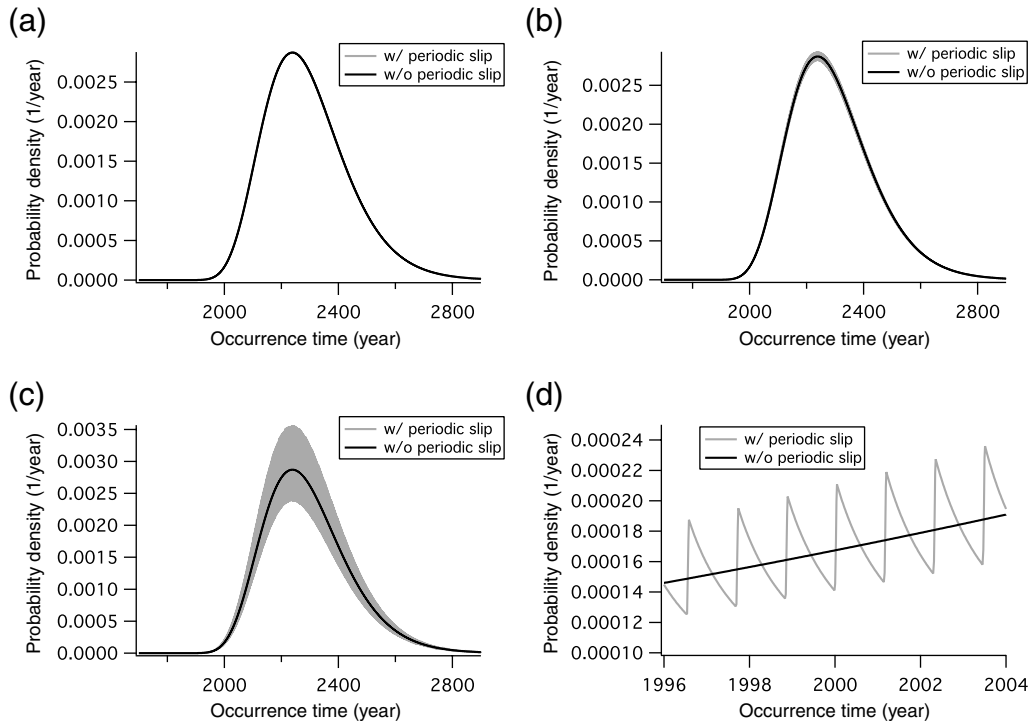


Figure 6. Comparison of the expected probability of a great Cascadia earthquake, assuming a delayed failure relation in equation (2), with $a = 0.008$ and subject to constant (black line) and to periodic loading (gray line). (a) The inverse Gaussian probability density is shown, with mean of 592.5 years and standard deviation of 149.3 years (see caption of Fig. 5). The black line is the occurrence density, assuming constant loading rate of 0.0045 MPa/yr. The case in gray, which is essentially identical and is plotted beneath the constant stressing rate case, assumes periodic loading with a fast rate of 0.089 MPa/year for two weeks, interevent slow loading at 0.00167 MPa/yr for 58 weeks, and an effective normal stress of 100 MPa. (b) The probability density using the same input values as shown in (a), except the effective normal stress is 10 MPa. (c) The probability density using the same input values as shown in (a), except the effective normal stress is 1 MPa. (d) The probability density shown in (c) but at an expanded scale to better illustrate the amplitude and time dependence for comparison with the result shown in Figure 5a.

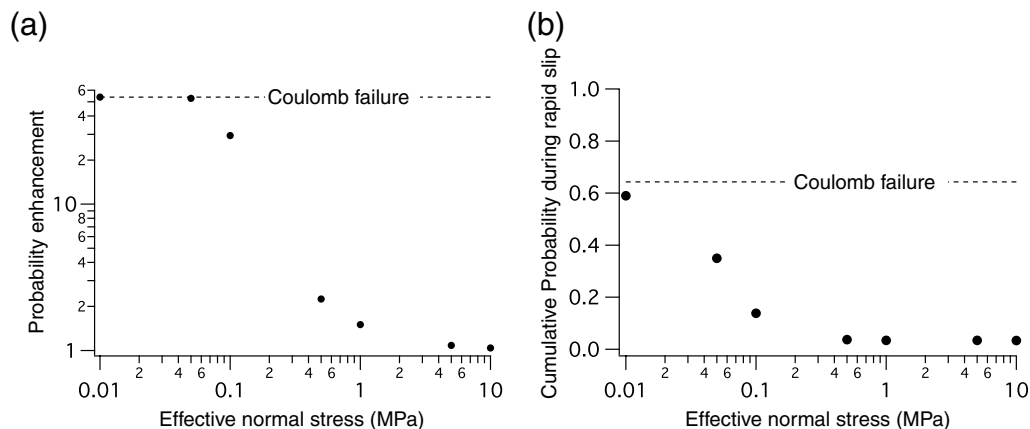


Figure 7. Summary of the delayed failure results. (a) Maximum probability enhancement during a rapid slip event, calculated with the delayed failure relation in equation (2) with $a = 0.008$ at a range of normal stresses between 10 kPa and 10 MPa. This is a plot of the ratio of the maximum probability density observed during a rapid slip event to the minimum probability density observed during the subsequent interevent period. This ratio is the maximum probability enhancement resulting from rapid slip. Shown for reference is the Coulomb failure result (an enhancement of $\sim 53\times$). (b) The cumulative probability during rapid slip P_{rapid} (see text) as a function of normal stress, for the same calculations as shown in (a). P_{rapid} is the probability that the next great Cascadia earthquake will occur during a rapid slip event, as opposed to during the rapid slip interevent period. Only when the effective normal stresses is less than 50 kPa is P_{rapid} greater than 50%.

considering the occurrence of seismicity in Cascadia, in subduction zones and elsewhere, and we present evidence from natural seismicity in support of that contention. We then consider existing constraints on the effective normal stress in the hypocentral region of great Cascadia earthquakes, as well as more generally for the locked portions of subduction zones, and argue that the *in situ* effective normal stresses are of the order of 1 MPa or greater.

Which Failure Relation?

As discussed briefly in the [Introduction](#), laboratory observations of intact rock failure and stick-slip sliding on pre-existing faults do not obey threshold failure; instead, failure invariably depends on time in some way. In rock failure tests, this is evident principally as static fatigue in which time of failure depends on the absolute stress level (e.g., [Scholz, 1972](#); [Kranz, 1980](#); [Fig. 3](#)). Other time-dependent manifestations of delayed failure such as precursory slip are obvious in stick-slip sliding tests (e.g., [Dieterich, 1992](#); [Fig. 4](#)). Both static fatigue and precursory slip arise from underlying physical mechanisms such as subcritical crack growth and dislocation glide ([Beeler et al., 2007](#)) that are manifest as a small positive, nonlinear, instantaneous dependence of fault strength on sliding rate, the $a \ln V/V_*$ term in equation (2a). This instantaneous rate dependence is observed in all low-temperature rock deformation experiments, including friction ([Dieterich, 1979](#)), fracture ([Scholz, 1968](#)), crack growth ([Atkinson and Meredith, 1987a, b](#)), and plasticity ([Mares and Kronenberg, 1993](#)). These observations suggest that delayed failure is the expected behavior, regardless of depth, temperature, and pressure within the Earth's crust.

More compelling than laboratory data, natural seismicity also displays evidence to distinguish between threshold and delayed failure. The appropriate failure relationship for earthquake probability calculations can be inferred from the observed response of earthquake failure times to variable natural stresses. Tidal forces exerted by the moon and sun produce continuously varying stresses in the Earth's crust with daily maximum shear-stressing rates that are two orders of magnitude larger than the daily rate of accumulation of stress along active faults due to plate motion ([Heaton, 1982](#)). There is a very short daily time window in which faults are subjected to stress levels higher than in the previous tidal cycle and relatively long periods in which the stress is decreasing. If faults failed at a Coulomb threshold stress, all earthquakes would occur when the stress was increasing and at stress levels not seen in the previous cycle, and all virtually earthquake occurrence would correlate with the Earth tides (e.g., [Heaton, 1982](#); [Lockner and Beeler, 1999](#)). Because earthquakes occur at all phases of the tides, including the times when the stress is decreasing, threshold models are an inappropriate failure model for calculating the effect of stress change on earthquake probability ([Knopoff, 1964](#); [Heaton, 1982](#); [Rydelek and Hass, 1994](#)).

Although it is clear that the timing of most earthquakes is not controlled by the tides, it has been shown statistically that some earthquake populations are influenced by the tides. In locations where the tidally induced stresses are especially large, a correlation is easier to detect. Recognizing this dependence on amplitude, [Wilcock \(2001\)](#), studied earthquakes on the Endeavor segment of the Juan de Fuca Ridge where the ocean tidal stress amplitudes are tens of kPa; this is ten or more times higher than the solid earth tidal amplitude. [Wilcock \(2001\)](#) found statistically significant tidal triggering in an earthquake catalog with ~ 1500 earthquakes. Following the same approach, [Cochran et al. \(2004\)](#) found a statistically significant correlation with ocean tidal amplitudes of > 20 kPa in a population of 20 thrust earthquakes, the degree of correlation decreasing systematically as the tidal amplitude decreases. Consistent with these demonstrations of an amplitude sensitivity, typical earth tide amplitudes (1–4 kPa) require much larger datasets to detect a statistically significant correlation. Using a California catalog with greater than 13,000 events, [Vidale et al. \(1998\)](#) found no significant correlation with the solid Earth tides, whereas using a worldwide catalog of $> 440,000$ events between 1973 and 2007, [Métivier et al. \(2009\)](#) detected a weak correlation, finding that $\sim 1\%$ of earthquakes correlate with the earth tides. Similarly, [Tanaka et al. \(2004\)](#) report correlation with the combined earth and oceanic tides in some regions in Japan. Their results are somewhat difficult to compare, but they are consistent with [Vidale et al. \(1998\)](#) and [Métivier et al. \(2009\)](#) in that the catalog is large ($> 89,000$ events) and the correlation is weak. [Tanaka et al. \(2004\)](#) divided Japan into 100 subregions each with > 200 earthquakes and found 13 subregions with a tidal correlation. One difference with the previous studies is that within the 13 subregions they estimate that approximately 10% of the earthquakes correlate with the tides, about 10 times that seen by [Métivier](#). However, because these are only 13% of the 100 subregions, fewer than 10% and possibly as few as 1.3% of the total population are correlated with the tides. This is fairly consistent with the 1% found by [Métivier et al. \(2009\)](#) especially because [Tanaka et al. \(2004\)](#) include the ocean tides, which are larger than the Earth tides, implying larger amplitudes than in the [Vidale et al. \(1998\)](#) and [Métivier et al. \(2009\)](#) studies.

Delayed failure generally explains the above observations. For delayed failure (equations 2a and 2b) the number of events N necessary to detect tidal triggering is

$$N \approx \frac{-\ln P_{rw}}{\left(\frac{\Delta\tau}{2a\sigma_c}\right)^2}, \quad (3)$$

in which $\Delta\tau$ is the amplitude of the periodic stress, and P_{rw} is the probability that the population is not correlated ([Beeler and Lockner, 2003](#)). Using equation (3) for typical solid earth tidal amplitudes and crustal stress conditions, detecting the correlation with the tides at the 95% confidence level would require tens of thousands of events ([Beeler and Lockner, 2003](#)). On the basis of an extrapolation of delayed failure

Table 2
Compiled Great Earthquake Stress Drops

Date (yyyy/mm/dd)	Location	M_w	Stress Drop (MPa)	Citation
1960/05/22	Chile	9.5	0.85	Barrientos and Ward (1990)
1964/05/28	Alaska	9.2	2.8	Kanamori (1970)
2004/12/26	Sumatra	9.1	6.0	Sorensen <i>et al.</i> (2005)
1952/04/11	Kamchatka	9.0	0.8*	Bath and Benihoff (1958)
2011/03/03	Japan	9.0	15	Kanamori (2011)

*Stress drop for the 1952 Kamchatka earthquake is from Bath and Benihoff (1958) estimated average slip D of 5 m, rupture width W of 240 km, assumed shear modulus $G = 60$ MPa and the relationship of Knopoff (1958) $\Delta\tau_s = D2G/\pi W$.

in laboratory experiments, Lockner and Beeler (1999) estimated approximately 1% of natural earthquakes would correlate with the solid earth tides. Note that with the exception of Vidale *et al.* (1998), who found no statistically significant relation between the earth tides and earthquakes, the Lockner and Beeler (1999) prediction preceded all the above cited studies finding correlation of natural earthquake occurrence and tidal stresses, in particular prior to Métivier *et al.* (2009) by a decade. Equation (3) shows a strong and nonlinear dependence on the stress amplitude, consistent with Wilcock (2001) and Cochran *et al.* (2004). There is also a strong sensitivity of equation (3) to effective normal stress; the expectation being that regions of the Earth's crust that have elevated pore fluid pressure would show anomalous tidal correlation. In his follow-up study of tidal triggering of earthquakes in the northeast Pacific Ocean, where the ocean tidal amplitudes are large, Wilcock (2009) found strong qualitative agreement with delayed failure but a stronger sensitivity to the tides than a strict reading of equation (3) assuming hydrostatic fluid pressure; his tentative interpretation of these results is that triggering is either stronger than evident in the laboratory data of Lockner and Beeler (1999) or that pore pressure is elevated in this region.

An additional key prediction of delayed failure is the occurrence of earthquakes at all phases of the tidal stress, with the maximum rate of earthquake occurrence coinciding with the maximum in friction ($f = \tau/\sigma_e$). Instantaneous failure requires correlation with the maximum stressing rate not seen in previous tidal cycles, no occurrence during periods of decreasing stress, and no occurrence at stress levels experienced in previous tidal cycles (Lockner and Beeler, 1999). In a normal-faulting environment, Wilcock (2001) examined the relation between earthquake occurrence and phase of the tidal stress and found the maximum earthquake occurrence rate coincident with the maximum extensional tidal stress. Similarly, Cochran *et al.* (2004) found the maximum rate of occurrence coincided with the friction maximum. These results are entirely consistent with delayed failure.

Hypocentral Effective Normal Stress

If equation (3) is used to consider the effective normal stress for large subduction zone earthquakes and the effective

normal stress were as low as 1 MPa, taking a tidal stress amplitude of 3 kPa, $a = 0.008$, and $P_{rw} = 0.05$ (95% confidence that the population of earthquakes is correlated), then $N = 85$, and tidal triggering of earthquakes would be obvious even in limited earthquake catalogs. Discounting nonvolcanic tremor, to date no evidence suggests that earthquakes in Cascadia in the vicinity of the subduction interface are correlated with the earth or oceanic tides, nor does this seem to be true in other subduction zones, suggesting that effective normal stresses in the hypocentral regions of subduction zones that host great earthquakes are higher than 1 MPa. Though many studies of the mechanics of subduction zones argue for near-lithostatic pore pressure (e.g., Wang and He, 1994), regardless of the choice of failure model, we believe it is unlikely that effective stress in the coseismic region is as low as 1 MPa. For a cohesionless fault, the shear resistance is given by $\tau = f\sigma_e$. Friction coefficients at significant depth in the crust range from around 0.65 for quartzofeldspathic rocks (Byerlee, 1978) to 0.1 for talc. If the minimum shear resistance of a seismic fault is the stress drop, then we can estimate minimum effective normal stress as $\sigma_e = \Delta\tau_s/f$. Because there have been no instrumentally recorded great earthquakes in Cascadia we must use stress drops from worldwide great subduction zone earthquakes as a proxy. These range from 0.80 to 15 MPa (Table 2), suggesting typical stress drops and producing minimum effective normal stresses of 1.2–150 MPa; caveats are the small sample size and the crude nature of many of the estimated stress drops. For comparison, Allmann and Shearer (2009) find a median stress drop of ~ 3 MPa for $>M 5$ subduction zone earthquakes.

Another approach for estimating the minimum effective normal stress is to use the lower bound on the average recurrence interval in Cascadia (Goldfinger *et al.*, 2012), $t_r = 500$ years, along with the stressing rate to estimate the typical earthquake stress drop in the locked zone, $\Delta\tau_s = t_r \dot{\tau}$. The stressing rate is the product of the average loading velocity, $V_L = 42$ mm/yr and the shear stiffness of the fault, k . If we use the formula in Knopoff (1958) for stiffness when fault length greatly exceeds width W , $k = 2G/\pi W$, $W = 90$ km (Flück *et al.*, 1997, note that these authors use a 60 km wide locked zone and a 60 km transition zone that has a spatially averaged coupling coefficient of 1/2), and $G = 30,000$ MPa, we calculate a stress drop of 4.5 MPa.

These attempts to estimate stress drop are in line with typical values so, if we conservatively use a typical subduction zone earthquake stress drop of 3 MPa (Allmann and Shearer, 2009) as the minimum shear stress prior to earthquake failure, again with $\sigma_e = \Delta\tau_s/f$ and $f = 0.65-0.1$, then the minimum effective normal stress ranges from 4.6 to 30 MPa.

A somewhat more sophisticated but still crude estimate of the minimum effective normal stress can be derived by accounting for the absolute stresses from the lithostatic load of overburden. Assuming Andersonian faulting (e.g., Wang and He, 1994) the relationship between the fault-normal stress σ_n and the lithostatic stress from overburden σ_L is

$$\sigma_n = \sigma_L + \frac{\tau(1 - \cos 2\phi)}{\sin 2\phi}, \quad (4)$$

in which ϕ is the dip angle of the fault. Taking ϕ to be in the range of $11.6^\circ-21.2^\circ$ (McCroory *et al.*, 2012) and again using a minimum shear stress given by a typical earthquake stress drop (3 MPa), we find the normal stress to be in the range $\sigma_n = \sigma_L + 0.56$ MPa to $\sigma_n = \sigma_L + 1.1$ MPa. The effective friction coefficient is $f' = f\sigma_e/\sigma_n$ so $\sigma_e = \sigma_n f'/f$. Wang and He (1994) find effective friction coefficients in the range of 0.05–0.09 for the Cascadia and Nankai subduction zones. Using these values and the same range of friction coefficients (0.1–0.65), along with a lithostatic load of 980 MPa (35 km depth with a lithostat of 28 MPa/km), gives a minimum effective normal stress of 75 MPa. Taking all of our estimations of the hypocentral effective normal stress in Cascadia into consideration, we propose the lower bound on the effective normal stresses is in the range of 1.3–30 MPa. This is liable to be an appropriate estimate for other subduction zones as well.

If normal stress is indeed in the range estimated above and failure is delayed, periodic deep slip does not have a significant effect on great earthquake probability. Although this is our favored interpretation, real observational constraints on the effective normal stress anywhere in the crust are hard to come by, and we are unaware of such constraints on stress in subduction zones.

Rationally Measuring Probability Increase

If a threshold failure model is used, great earthquake probability estimates can be considered high or low, depending on the interpretation; for an example of the range of possible interpretations of a single probability result, we use our representative calculation for threshold failure (see [Application to Earthquake Recurrence](#)). On one hand, the weekly probability is enhanced by more than 50 times during the rapid slip event. If this is taken as an estimated probability gain (e.g., Jordan and Jones, 2010), it could be interpreted as sufficient reason for an agency in charge of earthquake monitoring to issue a public statement or earthquake warning during rapid slip events; the GSC did issue a public statement during the 2007 rapid slip event. On the other hand, the

absolute weekly probability of a great Cascadia earthquake during a rapid slip event is extremely low at $\sim 0.03\%$, which might be interpreted as a good reason not to raise undue alarm. Our calculations with delayed failure produce small probability gains and remove this ambiguity unless the effective normal stress is extremely low. Moreover, rather than considering weekly misleading probability gains or the absolute probabilities that are at extreme ends of the spectrum of estimates, an intermediate statistic may be more useful for judging when to make public statements. One such approach is to consider whether it is more likely that a great earthquake will occur during the periods between rapid slip events or during rapid slip events. We calculate the cumulative probability for two week periods of rapid slip $P_{\text{rapid}}(t) = \int_{t_{\text{start}}}^{t_{\text{end}}} p(t)dt$, in which t_{start} and t_{end} are the starting and ending times of the period of rapid slip, respectively, and compare that result with the cumulative probability for the 58 week period between periods of rapid slip, $P_{\text{slow}}(t) = \int_{t_{\text{start}}}^{t_{\text{end}}} p(t)dt$. For delayed failure (3), because changes in loading rate produce slow changes in earthquake rate, any increase due to rapid slip persists into the interevent period (Fig. 6c). By examining our delayed failure model at a range of normal stresses (Fig. 7b), we find that unless effective normal stresses are less than 50 kPa, it is more likely that a great earthquake will occur during the rapid slip interevent period than during a rapid event. Because 50 kPa is orders of magnitude smaller than typical earthquake stress drops, this result further illustrates the argument that significant increases in great earthquake probability do not coincide with rapid slip events for our model.

Alternative Models of Triggered Failure and the Significance of the “Gap”

In the present study, we have assumed the only means by which deep rapid slip can affect the occurrence time of a great Cascadia earthquake is via static stress transfer—and a somewhat remote static transfer at that. Our model has no spatial dimension, so deep slip is coupled to stress in the hypocentral region using a constant elastic coefficient (the fault stiffness). Of course, virtually nothing is known of the mechanics of deep slip, and it is entirely possible that deep episodic slip is more intimately connected to the onset of great earthquakes and more directly triggers great earthquakes than we have estimated in our calculations. For example, if the amplitudes of successive deep slip events increase over time, the per-event stress transfer will increase. Even more alarming would be if deep slip becomes shallower over time, as this would cause the per-event stress transfer to increase dramatically. Static stresses decrease with distance, d , from the source as $\sim 1/d^3$, so small increases in the up-dip extent of deep slip would have a large effect. In such circumstances, deep episodic slip may act as a deep nucleation phase of the large earthquake rather than a remote static stress trigger as presumed in the calculations in this paper. Dimensioned, deterministic models of deep slip cycles that include propagation show this kind of nucleation triggering (Segall and

Bradley, 2010, 2012). This aspect could be incorporated into our model by allowing the stiffness that controls stress transfer from the deep slip to the locked zone to increase with time. However, in the Segall and Bradley models, all great earthquakes are continuations of periodic deep slip events, and therefore the implicit interevent probability is always zero. The differences in implied hazard between our spatially dimensionless probabilistic model and the Segall and Bradley (2010, 2012) well-dimensioned, deterministic model could hardly be larger, underscoring the need for real-time monitoring and analysis of location, magnitude, and up-dip extent of deep slip events in Cascadia and elsewhere where deep slip has been identified.

In the calculations conducted in this study and in the spatially dimensioned models of episodic deep slip (Segall and Bradley, 2010, 2012), the deep slip and locked zones are effectively adjacent to one another. For Segall and Bradley (2010) the two zones do not have distinct rheological or hydrological properties. The principal difference between the regions in their models is that there is low effective pressure in the deep slipping region, and high effective pressure in the locked region. Quite a different picture appears in Figure 1, in the related literature on the composition and mechanical properties of subduction zones (Wang *et al.*, 2011), in some studies of associated nonvolcanic tremor (Wech and Creager, 2008), and in some geodetic inversions for the locking depth in Cascadia (Burgette *et al.*, 2009). In that body of literature, there is an implied distinct separation, a gap, between the locked zone and the region of deep episodic slip. However, in other studies that locate nonvolcanic tremor (Wech and Creager, 2011), the tremor, and by interference slip, extend into this region.

A definitive but spatially limited constraint on the up-dip extent of episodic deep slip comes from the Plate Boundary Observatory (PBO) borehole strainmeters. These instruments have multiple gauges perpendicular to the borehole axis and record the full strain tensor parallel to the Earth's surface. The tensor strains can be converted to areal and engineering shear-strain components, and the character of the component signals associated with deep slip produce definitive information on the slip amplitude, propagation direction, and up-dip extent (Roeloffs *et al.*, 2009; Roeloffs and McCausland, 2010; E. A. Roeloffs and W. A. McCausland, unpublished manuscript, 2013). For four of the five deep slip events in northern Cascadia between 2007 and 2011, the up-dip limit of slip is tightly constrained to be approximately 50 km northeast of the down-dip limit of the 50% locked zone as inferred by Yoshioka *et al.* (2005) and McCaffrey *et al.* (2007). Slip as far up-dip as the probable base of the locked zone can be ruled out because, to reach the down-dip limit of the locked zone, slip would extend beneath the B004 strainmeter and produce a very distinct strain signal. On this basis, there is a 50 km "gap" between the base of the locked zone and the up-dip limit of deep slip events in northern Cascadia.

Gap or not, the rheological properties of the region immediately up-dip of the deep slip termination are impor-

tant for understanding the mechanical relation between deep slip and large earthquakes, and they are extremely important for assessing the seismic hazard. This region could either be locked, steadily slipping with rheological properties that are distinct from both the locked and episodic zones, or be a region of transition between locked and creeping, as often assumed in geodetic inversions for the locking depth (e.g., Yoshioka *et al.*, 2005; McCaffrey *et al.*, 2007; Burgette *et al.*, 2009). An intervening creeping zone will act to decouple stress transfer from deep episodic slip to the up-dip locked zone and reduce the probability that the great earthquake is directly triggered by deep slip. That will be true in models of the type used in the present study and in models of the type of Segall and Bradley (2010). The wider the up-dip creeping zone there is, the less coupled the stress transfer from deep slip will become and the smaller the probability that great earthquakes are directly triggered or nucleated by deep episodic slip. If, instead, the up-dip region is partially or fully locked, there would be an accumulating slip deficit to be either made up in great earthquakes or in subsequent creep events up-dip of the current episodic deep slip zone (Wech and Creager, 2011). Again, eventual up-dip slip would significantly increase the short-term great earthquake hazard, and detecting such slip (should it occur) is a high priority for monitoring.

Monitoring Deep Slip

To date, there is no evidence of significant changes in the total amount and extent of slip events in northern Cascadia over time. Both the GPS and borehole strain data are consistent with northern Cascadia deep slip events representing slip in the direction of plate convergence on the upper surface of the subducting Juan de Fuca plate. Like the nonvolcanic tremor, the slip fronts of these events propagate along the strike of the slab at 2–10 km/d. Five of these events were recorded by PBO borehole strainmeters from 2007 through 2011. The strain signals from the most recent four of these events are nearly identical except they indicate propagation stopping successively further south. The borehole strain data are consistent with slip extending to an up-dip depth limit of 28 km and with net slip of 15–33 mm (E. A. Roeloffs and W. A. McCausland, unpublished manuscript, 2013). The uncertainty in the amount of slip is attributable to uncertainty in strainmeter calibration; all four of these events have essentially the same amount of slip. The strainmeter resolution is such that a 20% difference in slip amplitude could be resolved.

For the delayed failure model, the parameters of a northern Cascadia deep slip event that most influence the amount and rate by which it loads the locked portion of the slab are the net slip, the up-dip depth limit of slip, and the slip speed (loading rate). For fixed net slip, the delayed failure model implies that changing the slip speed would not change earthquake occurrence probabilities, because the ratio of the slip duration to the relaxation time would be unchanged.

On the other hand, increasing the net slip, but not the slip rate, would increase the conditional probability during the slip event, because the increased loading rate decreases the relaxation time without decreasing the event duration.

Some Final Context

Following [Mazzotti and Adams \(2004\)](#), in our calculations we have used the periodic deep slip below Vancouver Island to estimate its effect on great earthquake occurrence times by assuming that great Cascadia earthquakes nucleate up-dip from this portion of the subduction zone. Because episodic deep slip occurs independently at locations in Cascadia other than beneath Vancouver Island ([Brudzinski and Allen, 2007](#); [Mazzotti, 2007](#); [Szeliga et al., 2008](#); [Roeloffs et al., 2009](#); S. Mazzotti, personal comm., 2009), allowing that the great earthquake nucleates elsewhere, our probabilities are overestimated, as has already been shown by [Mazzotti \(2007\)](#). Specifically, and for example, simply allowing for the episodic slip events to have spatial dimension and segmentation reduces the threshold model ~ 50 times probability increase to ~ 10 times ([Mazzotti, 2007](#)). Furthermore, Cascadia may be segmented with smaller M_w 8 events in southern Cascadia, with shorter recurrences of ~ 240 years ([Goldfinger et al., 2012](#)) interspersed between the great Cascadia events. Reasonably, segmentation of deep slip and segmentation of large earthquakes should be considered in revised probability estimates of the M_w 9 Cascadia events.

With regard to the choice of a used in our estimates, the larger the value of a , the more the calculated seismicity rate will deviate from the threshold failure result. Because a has been shown to increase approximately linearly with absolute temperature ([Nakatani, 2001](#)) as expected from reaction rate theory ([Nakatani, 2001](#); [Rice et al., 2001](#)), our value of a is likely the minimum. Consequently, our estimated probabilities are larger than if we had accounted for temperature dependence of a . Given geothermal gradients and the expected hypocentral depth of great earthquakes in Cascadia, a is expected to be three or more times larger than the value used here. Because larger values will produce an even more damped response, the following calculations are a conservative estimate of the effect of delayed failure on probability.

Conclusions

If earthquake failure is delayed, as it is in rock failure and stick-slip friction experiments, changes in loading rate have little effect on earthquake occurrence rates so long as the duration of the loading rate change is short relative to the fault's characteristic delay time. The delay time is proportional to effective normal stress. When this kind of failure relationship is applied to estimate the effect of periodic deep slip on great earthquake occurrence in Cascadia, we find the probability enhancement during rapid deep slip is negligible for effective normal stresses of 10 MPa or more and increases only by a factor of 1.5 for an effective normal stress of

1 MPa. Furthermore, the delayed response also causes the probability enhancement induced by increasing the loading rate to extend into the deep slip interevent period. A consequence is that it is more likely a great earthquake will occur between the periods of rapid deep slip than during them unless the effective normal stress is less than 50 kPa. We have argued that effective normal stress in the hypocentral region of great subduction zone earthquakes is higher than 1 MPa; this is equivocal speculation. Nevertheless, we conclude that great earthquake probability is not enhanced significantly during deep slip events.

Data and Resources

All data used in this paper came from published sources listed in the references. Unpublished work of Stephane Mazzotti, [Mazzotti \(2007\)](#) in the reference list is available at http://earthquake.usgs.gov/aboutus/nepec/meetings/07May_Portland/Presentations/NEPEC_051807_01_Rogers-Mazzotti_ETS.pdf (last accessed August 2012).

Acknowledgments

We are grateful to Stephane Mazzotti for sharing unpublished results, to Pat McCrory and Luke Blair for providing Cascadia subduction zone dip estimates, to Jim Dieterich for explaining his earthquake rate equations, and to Paul Reasenber for helping N.M.B. understand earthquake probability density and maximum likelihood estimates. Our knowledge of models of deep slip came from discussions with Allan Rubin, Paul Segall, and Jim Dieterich. Annemarie Baltay provided the references and suggested methods to estimate the large subduction earthquake stress drops. N.M.B. especially appreciates a long dialogue on tidal triggering of earthquakes and deep non-volcanic tremor with Amanda Thomas and Roland Burgmann, and another with David Lockner. This manuscript was greatly improved in response to reviews by Ross Stein and Bill Ellsworth of the U.S. Geological Survey and two anonymous BSSA referees. Ross provided estimates of the delayed failure time constant from the earthquake triggering literature.

References

- Adams, J. (1990). Paleoseismicity of the Cascadia subduction zone: Evidence from turbidites off the Oregon–Washington margin, *Tectonics* **9**, 569–583.
- Adams, J., and D. Weichert (1994). Near-term probability of the future Cascadia megquake, *U.S. Geol. Surv. Open-File Rept. 94-568*, 1–3.
- Allmann, B. B., and P. M. Shearer (2009). Global variations of stress drop for moderate to large earthquakes, *J. Geophys. Res.* **114**, doi: [10.1029/2008JB005821](https://doi.org/10.1029/2008JB005821).
- Atkinson, B. K., and P. G. Meredith (1987a). The theory of subcritical crack growth with applications to minerals and rocks, in *Fracture Mechanics of Rock*, B. K. Atkinson (Editor), Geol. Ser., Elsevier, New York, 111–166.
- Atkinson, B. K., and P. G. Meredith (1987b). Experimental fracture mechanics data for rocks and minerals, in *Fracture Mechanics of Rock*, B. K. Atkinson (Editor), Geol. Ser., Elsevier, New York, 477–525.
- Atwater, B. F. (1987). Evidence for great Holocene earthquakes along the outer coast of Washington State, *Science* **236**, 942–944.
- Atwater, B. F., and E. Hemphill-Haley (1997). Recurrence intervals for great earthquakes of the past 3,500 years at northeastern Willapa Bay, Washington, *U.S. Geological Survey Professional Paper 1576*, 108 pp.
- Barrientos, S. E., and S. N. Ward (1990). The 1960 Chile earthquake: Inversion for slip distribution from surface deformation, *Geophys. J. Int.* **103**, 589–598.

- Bath, M., and H. Benioff (1958). The aftershock sequence of the Kamchatka earthquake of November 4, 1952, *Bull. Seismol. Soc. Am.* **48**, 1–15.
- Beeler, N. M. (2004). Review of the physical basis of laboratory-derived relationships for brittle failure and their implications for earthquake nucleation and earthquake occurrence, *Pure Appl. Geophys.* **161**, 1853–1876.
- Beeler, N. M., and D. A. Lockner (2003). Why earthquakes correlate weakly with Earth tides: The effects of periodic stress on the rate and probability of earthquake occurrence, *J. Geophys. Res.* **108**, doi: [10.1029/2001JB001518](https://doi.org/10.1029/2001JB001518).
- Beeler, N. M., T. E. Tullis, A. K. Kronenberg, and L. A. Reinen (2007). The instantaneous rate dependence in low temperature laboratory rock friction and rock deformation experiments, *J. Geophys. Res.* **112**, doi: [10.1029/2005JB003772](https://doi.org/10.1029/2005JB003772).
- Brudzinski, M., and R. M. Allen (2007). Segmentation in episodic tremor and slip all along Cascadia, *Geology* **35**, 907–910.
- Burgette, R. J., R. J. Weldon II, and D. A. Schmidt (2009). Interseismic uplift rates for western Oregon and along strike variation in locking on the Cascadia subduction zone, *J. Geophys. Res.* **114**, doi: [10.1029/2008JB005679](https://doi.org/10.1029/2008JB005679).
- Byerlee, J. D. (1978). Friction of rocks, *Pure Appl. Geophys.* **116**, 615–626.
- Cochran, E. S., J. E. Vidale, and S. Tanaka (2004). Earth tides can trigger shallow thrust fault earthquakes, *Science* **306**, 1164–1166.
- Dieterich, J. H. (1979). Modeling of rock friction: 1. Experimental results and constitutive equations, *J. Geophys. Res.* **84**, 2161–2168.
- Dieterich, J. H. (1992). Earthquake nucleation on faults with rate- and state-dependent strength, in *Earthquake Source Physics and Earthquake Precursors*, T. Mikumo (Editor), Elsevier, New York, 115–134.
- Dieterich, J. H. (1994). A constitutive law for rate of earthquake production and its application to earthquake clustering, *J. Geophys. Res.* **99**, 2601–2618.
- Dieterich, J. H., and B. Kilgore (1996). Implications of fault constitutive properties for earthquake prediction, *Proc. Natl. Acad. Sci. USA* **93**, 3787–3794.
- Dragert, H., R. D. Hyndman, G. C. Rogers, and K. Wang (1994). Current deformation and the width of the seismogenic zone of the northern Cascadia subduction thrust, *J. Geophys. Res.* **99**, 653–668.
- Dragert, H., K. Wang, and T. S. James (2001). A silent slip event on the deeper Cascadia subduction interface, *Science* **292**, 1525–1528.
- Flück, P., R. D. Hyndman, and K. Wang (1997). Three-dimensional dislocation model for great earthquakes of the Cascadia subduction zone, *J. Geophys. Res.* **102**, 20,539–20,550.
- Frankel, A. D., and M. D. Petersen (2008). Cascadia subduction zone, Appendix L, in *The Uniform California Earthquake Rupture Forecast*, version 2 (UCERF 2), *U.S. Geological Survey Open-File Report 2007-1437L and California Geological Survey Special Report 203L*, 7 pp.
- Goldfinger, C., C. H. Nelson, and J. E. Johnson (2003). Holocene earthquake records from the Cascadia subduction zone and northern San Andreas Fault based on precise dating of offshore turbidites, *Ann. Rev. Earth Planet. Sci.* **31**, 555–577.
- Goldfinger, C., C. H. Nelson, A. E. Morey, J. R. Johnson, J. Patton, E. Karabanov, J. Gutierrez-Pastor, A. T. Eriksson, E. Gracia, G. Dunhill, R. J. Enkin, A. Dallimore, and T. Vallier (2012). Turbidite event history—Methods and implications for Holocene paleoseismicity of the Cascadia subduction zone, *U.S. Geol. Surv. Prof. Paper 1661-F*, 170 pp.
- Hardebeck, J. L. (2004). Stress triggering and earthquake probability estimates, *J. Geophys. Res.* **109**, doi: [10.1029/2003JB002437](https://doi.org/10.1029/2003JB002437).
- Heaton, T. H. (1982). Tidal triggering of earthquakes, *Bull. Seismol. Soc. Am.* **72**, 2181–2200.
- Jordan, T. H., and L. M. Jones (2010). Operational earthquake forecasting: Some thoughts on why and how, *Seismol. Res. Lett.* **81**, 577, doi: [10.1785/gssrl.81.4.571](https://doi.org/10.1785/gssrl.81.4.571).
- Kanamori, H. (1970). The Alaska earthquake of 1964: Radiation of long-period surface waves and source mechanism, *J. Geophys. Res.* **75**, 5029–5040.
- Kanamori, H. (2011). The 2011 Tohoku-oki earthquake—overview, *Seismol. Res. Lett.* **82**, 441.
- Kilgore, B., and N. M. Beeler (2010). Evaluating earthquake ‘predictions’ on laboratory experiments and resulting strategies for ‘predicting’ natural earthquake recurrence, *Seismol. Res. Lett.* **81**, 361.
- Knopoff, L. (1958). Energy release in earthquakes, *Geophys. J. Roy. Astron. Soc.* **1**, 44–52.
- Knopoff, L. (1964). Earth tides as a triggering mechanism for earthquakes, *Bull. Seismol. Soc. Am.* **54**, 1865–1870.
- Kranz, R. L. (1980). The effects of confining pressure and stress difference on static fatigue of granite, *J. Geophys. Res.* **85**, 1854–1866.
- Leonard, L., R. D. Hyndman, and S. Mazzotti (2004). Coseismic subsidence in the 1700 great Cascadia earthquake: Geological estimates versus geodetically controlled elastic dislocation models, *Geol. Soc. Am. Bull.* **116**, doi: [10.1130/B25369.1](https://doi.org/10.1130/B25369.1).
- Lockner, D. A., and N. M. Beeler (1999). Premonitory slip and tidal triggering of earthquakes, *J. Geophys. Res.* **104**, 20,133–20,151.
- Mares, V. M., and A. K. Kronenberg (1993). Experimental deformation of muscovite, *J. Struct. Geol.* **15**, 1061–1075.
- Mazzotti, S. (2007). A review of episodic tremor and slip (ETS): Observations in the northern Cascadia subduction zone and hazard implications, presentation to the *National Earthquake Prediction Council (NEPEC)*, Portland, Oregon, 5 May 2007.
- Mazzotti, S., and J. Adams (2004). Variability of near-term probability for the next great earthquake on the Cascadia subduction zone, *Bull. Seismol. Soc. Am.* **94**, 1954–1959.
- Mazzotti, S., H. Dragert, J. Henton, M. Schmidt, R. Hyndman, T. James, Y. Lu, and M. Craymer (2003). Current tectonics of northern Cascadia from a decade of GPS measurements, *J. Geophys. Res.* **108**, doi: [10.1029/2003JB002653](https://doi.org/10.1029/2003JB002653).
- McCaffrey, R., M. D. Long, C. Goldfinger, P. C. Zwick, J. L. Nabelek, and C. K. Johnson (2000). Rotation and plate locking at the southern Cascadia subduction zone, *Geophys. Res. Lett.* **27**, 3117–3120, doi: [10.1029/2000GL011768](https://doi.org/10.1029/2000GL011768).
- McCaffrey, R., A. I. Qamar, R. W. King, R. Wells, G. Khazaradze, C. A. Williams, C. W. Stevens, J. J. Vollick, and P. C. Zwick (2007). Fault locking, block rotation and crustal deformation in the Pacific Northwest, *Geophys. J. Int.* **169**, 1315–1340, doi: [10.1111/j.1365-246X.2007.03371.x](https://doi.org/10.1111/j.1365-246X.2007.03371.x).
- McCausland, W., S. Malone, and D. Johnson (2005). Temporal and spatial occurrence of deep non-volcanic tremor: From Washington to northern California, *Geophys. Res. Lett.* **32**, doi: [10.1029/2005GL024349](https://doi.org/10.1029/2005GL024349).
- McCrory, P. A., J. L. Blair, F. Waldhauser, and D. H. Oppenheimer (2012). Juan de Fuca slab geometry and its relation to Wadati-Benioff zone seismicity, *J. Geophys. Res.* **117**, doi: [10.1029/2012JB009407](https://doi.org/10.1029/2012JB009407).
- Métivier, L., O. de Viron, C. Conrad, S. Renaul, M. Diament, and G. Patau (2009). Evidence of earthquake triggering by the solid earth tides, *Earth Planet. Sci. Lett.* **278**, 370–375.
- Nakatani, M. (2001). Conceptual and physical clarification of rate and state friction: Frictional sliding as a thermally activated rheology, *J. Geophys. Res.* **106**, 13347–13380.
- Parsons, T. (2002). Global Omori law decay of triggered earthquakes: Large aftershocks outside the classical aftershock zone, *J. Geophys. Res.* **107**, doi: [10.1029/2001JB000646](https://doi.org/10.1029/2001JB000646).
- Parsons, T., S. Toda, R. S. Stein, A. Barka, and J. H. Dieterich (2000). Heightened odds of large earthquakes near Istanbul: an interaction-based probability calculation, *Science* **288**, 661–665.
- Petersen, M. D., A. D. Frankel, S. C. Harmsen, C. S. Mueller, K. M. Haller, R. L. Wheeler, R. L. Wesson, Y. Zeng, O. S. Boyd, D. M. Perkins, and N. Luco (2008). Documentation for the 2008 update of the United States national seismic hazard maps, *U.S. Geol. Surv. Open-File Rept. 2008-1128*, 60 pp.
- Rice, J. R., N. Lapusta, and K. Ranjith (2001). Rate and state dependent friction and the stability of sliding between elastically deformable solids, *J. Mech. Phys. Sol.* **49**, 1865–1898.
- Roeloffs, E. A., and W. A. McCausland (2010). Constraints on aseismic slip during and between northern Cascadia episodic tremor and slip events from PBO borehole strainmeters, *Seismol. Res. Lett.* **81**, 337.

- Roeloffs, E. A., P. G. Silver, and W. A. McCausland (2009). Transient strain during and between northern Cascadia episodic tremor and slip events from plate boundary observatory borehole strainmeters (abstract G12A-02), *Eos Trans. AGU* **90**, no. 22 (Joint. Assem. Suppl.), G12A-02.
- Rydelek, P. A., and L. Hass (1994). On estimating the amount of blasts in seismic catalogs with Schuster's method, *Bull. Seismol. Soc. Am.* **84**, 1256–1259.
- Satake, K., K. Shimazaki, Y. Tsuji, and K. Ueda (1996). Time and size of a giant earthquake in Cascadia inferred from Japanese tsunami record of January, 1700, *Nature* **379**, 246–249.
- Savage, J. C. (1991). Criticism of some forecasts of the National Earthquake Prediction Evaluation Council, *Bull. Seismol. Soc. Am.* **81**, 862–881.
- Schmidt, D. A., and H. Gao (2010). Source parameters and time-dependent slip distributions of slow slip events on the Cascadia subduction zone from 1998 to 2008, *J. Geophys. Res.* **115**, doi: [10.1029/2008JB006045](https://doi.org/10.1029/2008JB006045).
- Scholz, C. H. (1968). Microfractures, aftershocks and seismicity, *Bull. Seismol. Soc. Am.* **58**, 1117–1130.
- Scholz, C. H. (1972). Static fatigue in quartz, *J. Geophys. Res.* **77**, 2104–2114.
- Segall, P., and A. M. Bradley (2010). Numerical simulation of slow slip and dynamic rupture in the Cascadia Subduction Zone, Abstract S13D-05 presented at *2010 Fall Meeting, AGU*, San Francisco, California, 13–17 December 2010.
- Segall, P., and A. M. Bradley (2012). Slow-slip evolves into megathrust earthquakes in 2D numerical simulations, *Geophys. Res. Lett.* **39**, doi: [10.1029/2012GL052811](https://doi.org/10.1029/2012GL052811).
- Segall, P., E. K. Desmarais, D. Shelly, A. Miklius, and P. Cervelli (2006). Earthquakes triggered by silent slip events on kilauea volcano, Hawaii, *Nature* **442**, 71–74.
- Sorensen, M. B., K. Atakan, and N. Pulido (2005). Simulated strong ground motions for the great *M* 9.3 Sumara-Andaman earthquake of 26 December 2004, *Bull. Seismol. Soc. Am.* **97**, S139–S151.
- Stein, R. S., A. A. Barka, and J. H. Dieterich (1997). Progressive failure on the North Anatolian fault since 1939 by earthquake stress triggering, *Geophys. J. Int.* **128**, 594–604.
- Szeliga, W., T. Melbourne, M. Santillan, and M. Miller (2008). GPS constraints on 34 slow slip events within the Cascadia subduction zone, 1997–2005, *J. Geophys. Res.* **113**, doi: [10.1029/2007JB004948](https://doi.org/10.1029/2007JB004948).
- Tanaka, S., M. Ohtake, and H. Sato (2004). Tidal triggering of earthquakes in Japan related to the regional tectonic stress, *Earth Planets Space* **56**, 511–515.
- Toda, S., R. S. Stein, K. Richards-Dinger, and S. Bozkurt (2005). Forecasting the evolution of seismicity in southern California: Animations built on earthquake stress transfer, *J. Geophys. Res.* **110**, doi: [10.1029/2004JB003415](https://doi.org/10.1029/2004JB003415).
- Vidale, J. E., D. C. Agnew, M. J. S. Johnston, and D. H. Oppenheimer (1998). Absence of earthquake correlation with Earth tides: An indication of high preseismic fault stress rate, *J. Geophys. Res.* **103**, 24567–24572.
- Wang, K., and J. He (1994). Mechanics of low-stress forearcs: Nankai and Cascadia, *J. Geophys. Res.* **104**, 15191–15205.
- Wang, K., I. Wada, and J. He (2011). Thermal and petrologic environments of ETS (abstract T22B-01), *Eos Trans. AGU* **90**, no. 52 (Fall Meet. Suppl.), T22B-01.
- Wech, A. G., and K. C. Creager (2008). Automated detection and location of Cascadia tremor, *Geophys. Res. Lett.* **35**, L20302, doi: [10.1029/2008GL035458](https://doi.org/10.1029/2008GL035458).
- Wech, A. G., and K. C. Creager (2011). A continuum of stress, strength and slip in the Cascadia subduction zone, *Nature Geosci.* **4**, doi: [10.1038/NNGEO1215](https://doi.org/10.1038/NNGEO1215).
- Wilcock, W. S. (2001). Tidal triggering of microearthquakes on the Juan de Fuca Ridge, *Geophys. Res. Lett.* **28**, 3999–4002.
- Wilcock, W. S. (2009). Tidal triggering of earthquakes in the Northeast Pacific Ocean, *Geophys. J. Int.* **179**, 1055–1070.
- Witter, R. C., H. M. Kelsey, and E. Hemphill-Haley (2003). Great Cascadia earthquakes and tsunamis of the past 6700 years, Coquille River estuary, southern coastal Oregon, *Geol. Soc. Am. Bull.* **115**, 1289–1306.
- Working Group on California Earthquake Probabilities (2008). The Uniform California Earthquake Rupture Forecast, Version 2 (UCERF 2), *U.S.*

Geol. Surv. Open-File Rept. 2007-1437 and Calif. Geol. Surv. Spec. Rept. 203.

- Yoshioka, S., K. Wang, and S. Mazzotti (2005). Interseismic locking of the plate interface in the northern Cascadia subduction zone, inferred from inversion of GPS data, *Earth Planet. Sci. Lett.* **231**, 239–247.

Appendix A

Delayed Failure

To represent laboratory observations of time-dependent failure, fault strength can be described by equation (2a), repeated here:

$$\tau = \sigma_e \left(f_* + a \ln \frac{V}{V_*} - b \frac{\delta}{d_c} \right) \quad (\text{A1})$$

(Dieterich, 1992, 1994). δ is slip, σ_e is the effective normal stress; τ is shear stress in the direction of slip; V is slip rate; a and b are experimentally determined constants that are second-order relative to the nominal friction f_* ; V_* is a reference slip velocity; and d_c is a slip weakening distance.

Static Fatigue

In a static fatigue test, stress is raised to a particular level τ at time $t = 0$ and then held constant. This is equivalent to setting the temporal derivative of equation (A1) to zero. The resulting relation between shear stress and time of failure t_f is

$$\tau = \sigma_e \left[f_* + a \ln \left(\frac{t_f b V_*}{a d_c} \right) \right] \quad (\text{A2})$$

(Beeler, 2004). The slope of shear stress versus the logarithm of failure time from (A2) (Fig. 3) is the product $a\sigma_e \ln(10)$.

Constant Stressing Rate

To estimate the failure time resulting from constant stressing rate, we represent the interaction of the fault with the elastic surroundings using a single degree-of-freedom elastic spring, $\tau = k(\delta_L - \delta)$, in which k is the spring stiffness that represents the surroundings and δ_L is the imposed loading displacement. The solution of (A1) for failure time under constant rate loading can be obtained by equating the temporal derivative of (A1) to that of the spring equation and integrating to determine the relation between time to failure t_{ff} and slip speed:

$$V = \frac{\dot{\tau}}{\left(\frac{b\sigma_e}{d_c} - k \right) \left(1 - \exp\left[\frac{\dot{\tau} t_{ff}}{a\sigma_e} \right] \right)}, \quad (\text{A3})$$

(Dieterich, 1992). As pointed out by Dieterich (1992), for delayed failure (equation A1), knowing the sliding velocity and loading rate at any time determines the remaining time to failure. Note the relationship amongst time t , time to failure t_{ff} , and failure time t_f is $t_{ff} = t_f - t$.

To apply this delayed failure model to predict a change in failure time resulting from a change in stressing rate, impose a change from the initial stressing rate $\dot{\tau}_0$ to $\dot{\tau}_1$ at time $t = t_0$. That is, for a pending failure, sliding at V at $t = t_0$ and subsequently loaded at a constant stressing rate, there are two possible failure times: (1) t_f^0 is the failure time if the stressing rate remains constant at the same rate $\dot{\tau}_0$, or (2) t_f^1 is the failure time if the stressing rate is changed to $\dot{\tau}_1$ at $t = t_0$. In the latter case, the resulting failure time can be determined using two versions of equation (A3), one for each of the two possible failure times t_f^0 and t_f^1 . V is the initial condition for either solution and can be eliminated by equating the two versions of equation (A3). Rearranging to solve for the failure time due to the changed loading rate results in

$$t_f^1 = t_0 + \frac{a\sigma_e}{\dot{\tau}_1} \ln \left[1 - \frac{\dot{\tau}_1}{\dot{\tau}_0} + \frac{\dot{\tau}_1}{\dot{\tau}_0} \exp \frac{\dot{\tau}_1(t_f^0 - t_0)}{a\sigma_e} \right]. \quad (\text{A4})$$

Equation (A4) can be used to define the failure time distribution for a collection of faults with a known starting distribution of failure times, t_f^0 (Fig. 2a). As noted by Dieterich (1994), the new distribution of failure times, under the new loading rate $\dot{\tau}_1$, can be calculated without explicitly including the sliding velocity. Equation (A4) is also independent of the stress weakening parameter b and the slip-weakening distance d_c (Dieterich, 1994). With reference to Figure 2a, values of failure time t_f^0 (horizontal axis) for a population of earthquakes resulting from stressing at the constant initial rate are shown by the gray symbols. The failure times t_f^1 (open squares) are the same earthquake population in which the failure times have been changed due to the change in stressing rate at time t_0 .

Appendix B

Seismicity Rates with Delayed Failure

To determine how the seismicity rate of a population of faults changes in response to a change in loading rate note that a seismicity rate r is the time derivative of occurrence, $r = dn/dt_f$, in which n is the (integer) number of an individual earthquake within the overall earthquake population. For two different sets of failure times t_f^0 and t_f^1 , such as in our conceptual earthquake populations (Fig. 2), the related seismicity rates are $r_0 = dn/dt_f^0$ and $r_1 = dn/dt_f^1$. Combining these rates into a single equation, we have

$$r_1 = r_0 \frac{dt_f^0}{dt_f^1} \quad (\text{B1})$$

(Beeler and Lockner, 2003), which follows from Dieterich (1994). r_0 is the background earthquake rate that would have resulted had there been no change in stressing rate. Estimating the response of seismicity rate to changes in stressing rate for the delayed failure model (equation A1) amounts to specifying the initial seismicity rate r_0 and calculating

dt_f^1/dt_f^0 . This derivative is the change in failure time due to a loading rate change, with respect to the failure time in the absence of a change in loading rate. The derivative can be obtained by differentiation of equation (A4). Substituting the result in equation (B1) yields

$$r_1(t_f^1) = r_0 \frac{\exp \frac{(t_f^1 - t_0)}{t_a}}{1 - \frac{\dot{\tau}_0}{\dot{\tau}_1} + \frac{\dot{\tau}_0}{\dot{\tau}_1} \exp \frac{(t_f^1 - t_0)}{t_a}}, \quad (\text{B2})$$

in which the characteristic time $t_a = a\sigma_e/\dot{\tau}_1$. Equations (A4) and (B2) are closely related to equation (3) of Segall *et al.* (2006). Figure 2b shows the nature of the seismicity rate response to a change in stressing rate. The seismicity rate evolves gradually and eventually approaches the steady-state value $r_0\dot{\tau}_1/\dot{\tau}_0$ over a few relaxation times t_a .

Appendix C

Seismicity Rates with Time Varying Background Rate

Time varying seismicity can be considered by allowing r_0 in equation (B1) to vary with time. In the case of earthquake recurrence, such as for great Cascadia earthquakes, we have a probabilistic representation of the earthquake recurrence time (Mazzotti and Adams, 2004), a density function with average recurrence and variance. An earthquake rate is related to probability density $p(t)$ as $r(t) = n_T p(t)$, in which n_T is the total number of earthquakes in the population. For a recurring earthquake, t is the recurrence interval t_r and the probability density must satisfy $n_T = \int_0^\infty p(t_r) dt_r = 1$. So, for earthquake recurrence, the seismicity rate describing possible failure times and the probability density of recurrence times are equivalent: $r(t_r) = p(t_r)$. In the following analysis, we represent the earthquake probability density for Cascadia recurrence intervals with an inverse Gaussian distribution,

$$p(t_r) = \sqrt{\frac{\gamma}{2\pi t_r^3}} \exp \left(\frac{-\gamma(t_r - \mu)^2}{2\mu^2 t_r} \right), \quad (\text{C1})$$

in which μ is the average recurrence interval and γ is a shape factor. The standard deviation s of the distribution is $s = \sqrt{\mu^3/\gamma}$. The inverse Gaussian is an arbitrary choice, and our eventual conclusions do not depend on the choice of density function.

Threshold Failure

As noted in the [Estimating the Effect of Changing Loading Rate on Earthquake Occurrence](#) section in the main text of this paper, for threshold failure, changes in seismicity rate are given by the change in stressing rate. Specifically for a change in stressing rate from $\dot{\tau}_0$ to $\dot{\tau}_1$ at recurrence time t_0 , the probability density distribution is

$$\begin{aligned}
p_0(t_r) &= \sqrt{\frac{\gamma}{2\pi t_r^3}} \exp\left(\frac{-\gamma(t_r - \mu)^2}{2\mu^2 t_r}\right) t_r < t_0 \\
p_1(t_r) &= \sqrt{\frac{\gamma}{2\pi t_r^3}} \exp\left(\frac{-\gamma(t_r - \mu)^2}{2\mu^2 t_r}\right) \frac{\dot{\tau}_1}{\dot{\tau}_0} t_r \geq t_0.
\end{aligned} \tag{C2a}$$

For subsequent changes in stressing rate, for example for a change back to $\dot{\tau}_0$ from $\dot{\tau}_1$ at time t_1 the distribution is

$$\begin{aligned}
p_1(t_r) &= \sqrt{\frac{\gamma}{2\pi t_r^3}} \exp\left(\frac{-\gamma(t_r - \mu)^2}{2\mu^2 t_r}\right) \frac{\dot{\tau}_1}{\dot{\tau}_0} t_0 \geq t_r < t_1 \\
p_2(t_r) &= p_1(t_r) \frac{\dot{\tau}_0}{\dot{\tau}_1} = \sqrt{\frac{\gamma}{2\pi t_r^3}} \exp\left(\frac{-\gamma(t_r - \mu)^2}{2\mu^2 t_r}\right) t_r \geq t_1.
\end{aligned} \tag{C2b}$$

Periodic changes in stressing rate can be calculated by successive application of (C2b), resulting in the distributions shown in Figure 5 (see text for discussion).

Delayed Failure

In the event the background seismicity rate is time varying, for delayed failure the resulting seismicity rate is

$$r_1(t_r^1) = r_0(t_r^0) \frac{\exp\left(\frac{t_r^1 - t_0}{t_a}\right)}{1 - \frac{\dot{\tau}_0}{\dot{\tau}_1} + \frac{\dot{\tau}_0}{\dot{\tau}_1} \exp\left(\frac{t_r^1 - t_0}{t_a}\right)}. \tag{C3}$$

Note that both failure timescales t_f^0 and t_f^1 appear in (C3). The mapping between failure timescales is given by equation (A4). The probability density distribution for the failure model of equation (A1) is given by substituting the density function (C1) into (C3):

$$\begin{aligned}
p_0(t_r^0) &= \sqrt{\frac{\gamma}{2\pi (t_r^0)^3}} \exp\left(\frac{-\gamma(t_r^0 - \mu)^2}{2\mu^2 t_r^0}\right) t_r^0 < t_0 \\
p_1(t_r^1) &= \sqrt{\frac{\gamma}{2\pi (t_r^0)^3}} \exp\left(\frac{-\gamma(t_r^0 - \mu)^2}{2\mu^2 t_r^0}\right) \\
&\quad \times \frac{\exp\left(\frac{t_r^1 - t_0}{t_a}\right)}{1 - \frac{\dot{\tau}_0}{\dot{\tau}_1} + \frac{\dot{\tau}_0}{\dot{\tau}_1} \exp\left(\frac{t_r^1 - t_0}{t_a}\right)} t_r^1 \geq t_0.
\end{aligned} \tag{C4a}$$

Again, note there are two recurrence timescales in the second of the equations in (C4a). t_r^0 is the time associated with the initial stressing rate, and t_r^1 is associated with the second stressing rate. Mapping between t_r^0 and t_r^1 is given by replacing t_f^0 and t_f^1 with t_r^0 and t_r^1 , respectively, in equation (A4).

For subsequent changes in stressing rate, for example for a change back to $\dot{\tau}_0$ from $\dot{\tau}_1$ at time t_1 ,

$$\begin{aligned}
p_1(t_r^1) &= \sqrt{\frac{\gamma}{2\pi (t_r^0)^3}} \exp\left(\frac{-\gamma(t_r^0 - \mu)^2}{2\mu^2 t_r^0}\right) \\
&\quad \times \frac{\exp\left(\frac{\dot{\tau}_1(t_r^1 - t_0)}{a\sigma_e}\right)}{1 - \frac{\dot{\tau}_0}{\dot{\tau}_1} + \frac{\dot{\tau}_0}{\dot{\tau}_1} \exp\left(\frac{\dot{\tau}_1(t_r^1 - t_0)}{a\sigma_e}\right)} t_0 \geq t_r^1 < t_1 \\
p_2(t_r^2) &= p_1(t_r^1) \frac{\exp\left(\frac{\dot{\tau}_0(t_r^2 - t_1)}{a\sigma_e}\right)}{1 - \frac{\dot{\tau}_1}{\dot{\tau}_0} + \frac{\dot{\tau}_1}{\dot{\tau}_0} \exp\left(\frac{\dot{\tau}_0(t_r^2 - t_1)}{a\sigma_e}\right)} t_r^2 \geq t_1.
\end{aligned} \tag{C4b}$$

Periodic changes in stressing rate can be calculated from recursive application of (C4b), resulting in distributions shown in Figure 6 (see text for Discussion).

U.S. Geological Survey
 Cascades Observatory
 1300 Cardinal Court
 Bldg. 10 Suite 100
 Vancouver, Washington 98683

Manuscript received 21 January 2012;
 Published Online 26 November 2013